

Experimental comparisons between one-part and normal (two-part) alkali-activated slag binders

Ren, Jie; Sun, Hongfang ; Li, Qun ; Li, Zhenming; Ling, Li ; Zhang, Xiaogang ; Wang, Yanshuai ; Xing, Feng

DOI

[10.1016/j.conbuildmat.2021.125177](https://doi.org/10.1016/j.conbuildmat.2021.125177)

Publication date

2021

Document Version

Accepted author manuscript

Published in

Construction and Building Materials

Citation (APA)

Ren, J., Sun, H., Li, Q., Li, Z., Ling, L., Zhang, X., Wang, Y., & Xing, F. (2021). Experimental comparisons between one-part and normal (two-part) alkali-activated slag binders. *Construction and Building Materials*, 309, 1-10. Article 125177. <https://doi.org/10.1016/j.conbuildmat.2021.125177>

Important note

To cite this publication, please use the final published version (if applicable). Please check the document version above.

Copyright

Other than for strictly personal use, it is not permitted to download, forward or distribute the text or part of it, without the consent of the author(s) and/or copyright holder(s), unless the work is under an open content license such as Creative Commons.

Takedown policy

Please contact us and provide details if you believe this document breaches copyrights. We will remove access to the work immediately and investigate your claim.

Experimental comparisons between one-part and normal (two-part) alkali-activated slag binders

Jie Ren^{1,*}, Hongfang Sun¹, Qun Li¹, Zhenming Li^{2,*}, Li Ling¹, Xiaogang Zhang¹, Yanshuai Wang¹, Feng Xing¹

¹ Guangdong Provincial Key Laboratory of Durability for Marine Civil Engineering, College of Civil and Transportation Engineering, Shenzhen University, Shenzhen 518060, China

² Department of Materials, Mechanics, Management & Design, Faculty of Civil Engineering and Geoscience, Delft University of Technology, Delft, the Netherlands

*Corresponding authors.

Abstract

One-part alkali-activated slag (AAS) binders are more promising in large-scale constructions because one-part mixing procedure is safer and easier to handle compared to normal two-part method. Thus, this study aims at investigating different properties of one-part AAS binders and control samples prepared using the two-part method. Experimental results of the former suggested the hardening time was greatly extended, but the workability showed little difference. Besides, compared to the control, one-part AAS binders had similar early compressive strength (within 7 days) and flexural strength in all tested curing stages but lower later compressive strength (from 28 days). The characterisation of the porous structures suggests that there were fewer C-A-S-H gels for one-part binders evidenced by less volume of mesopores but with larger amount of bigger pores. In addition, mineralogical and microstructural analyses imply that there was no hydrotalcite formed in the one-part AAS binders. Moreover, one-part AAS binders are more susceptible to efflorescence, presumably further affecting their surface and long-term durability.

Key words: One-part alkali-activated slag; Mechanical properties; Mineralogical and microstructural analysis; Pore microstructure; Efflorescence

1. Introduction

Traditional ordinary Portland cement (OPC) manufacturing is a major contributor to the global carbon dioxide emissions due to massive amount of CO₂ released from the calcination of limestone at 1400-1450 °C and corresponding intensive energy consumption involved. For instance, in 2016, the total CO₂ emission caused by the manufacturing of OPC was around 1.45

33 Gt, which was approximately 8% of the total anthropogenic CO₂ emissions [1]. Thus, many
34 researchers are seeking for alternative binders with low-carbon footprint [2-8]. Alkali-activated
35 slag (AAS) requires no heat curing and has a relatively higher early strength, low permeability
36 and stronger thermal stability as well as durability compared to OPC-based binders [4, 9-13].
37 However, the commonly-seen traditional activation process of AAS, also considered as two-
38 part mixing, involves preparation of concentrated alkaline solutions which are quite corrosive
39 and viscous, such as sodium (or potassium) hydroxide in particular. This is especially
40 inconvenient and unsafe for cast-in-situ large-scale applications.

41 One-part (also known as 'just add water') AAS binders are now gaining an increasing
42 attention from both academia and industrial sectors because they provide a safer and easier-to-
43 handle approach for wider applications of AAS binders compared to traditional two-part AAS
44 counterparts [14-17]. One-part AAS binders are prepared by simply adding water into a
45 mixture of slag, various types of solid activators and aggregates, similar to the preparation of
46 OPC-based binders. Apart from the advantages including safety and easy-to-handle approach,
47 one more advantage of using one-part mixing method for AAS binders is that it could to some
48 extent counteract the weakness of low-temperature mixing and curing such as subzero-
49 temperature concreting because low temperature could retard the hardening reactions of alkali-
50 activated materials [18, 19]. Specifically, when in contact with water, solid activators such as
51 sodium silicate or sodium hydroxide particles would release a large amount of heat, increasing
52 the temperature of whole mixtures. A few researches have already explored the viability of
53 one-part mixing method and corresponding properties of one-part AAS binders [14, 17, 20, 21].
54 Alzaza et al. [21] investigated the effects of low-temperature curing on the hardened properties
55 of one-part AAS and OPC-based binders. The results showed that although a lower curing
56 temperature would result in greater reduction in the compressive strength of mortars, the one-
57 part AAS binders achieved higher compressive strength compared to OPC-based counterparts.
58 Besides, after an extra room-temperature curing regime, the hardened properties of AAS could
59 be improved significantly. According to another study [14], the initial mixing water
60 temperature would influence the dissolution rate of solid activators. The experimental work
61 conducted by Luukkonen et al. [20] highlighted the importance of silica availability in
62 determining the fresh and hardened properties of one-part AAS binders. Despite of these
63 research, there is still some debate regarding various properties of AAS binders such as
64 compressive strength [22, 23], which might be due to a lack of systematic and comprehensive
65 investigation.

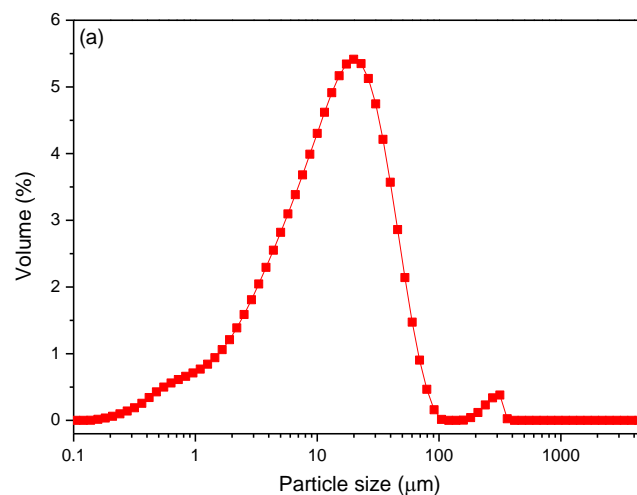
66 This study investigates the fresh and hardened properties of a type of one-part AAS binders,
67 including setting time, fluidity, hydration heat evolution, mechanical properties accompanied
68 with pore-related microstructures and mineralogical/microstructural characteristics. Reference
69 binders prepared with the same mixture proportion but using the normal (two-part) mixing
70 method were also made. The outcomes from this research are expected to enhance the technical
71 feasibility and commercial viability of AAS binders in related industries, especially for future
72 constructions in cold regions and countries.

73

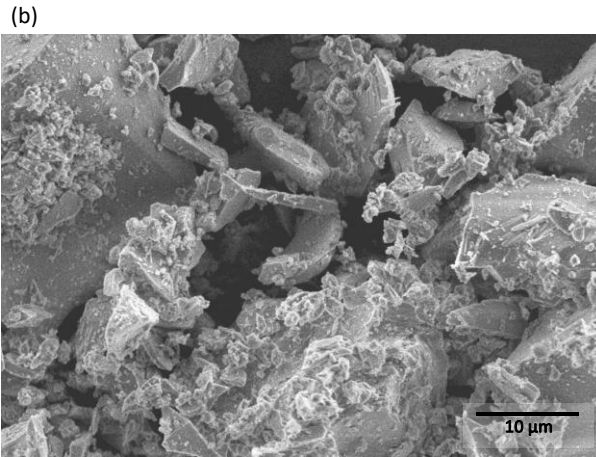
74 2. Experimental programme

75 2.1. Raw materials

76 The slag used in this study was granulated blast furnace slag (hereafter referred to as GBFS),
77 provided by Wuhan SinoCem Smartec Co., Ltd. Its specific density and Blaine fineness was
78 2900 kg/m^3 and $424 \text{ m}^2/\text{kg}$, respectively. The d_{10} , d_{50} and d_{90} of the GBFS used was 2.0, 12.5
79 and $38.4 \mu\text{m}$ accordingly with its particle size distribution and morphology shown in Fig. 1(a)
80 and (b). The chemical composition of GBFS is tabulated in Table 1. Anhydrous sodium
81 metasilicate (Na_2SiO_3) fine powders were employed as the solid activator with $\text{SiO}_2/\text{Na}_2\text{O}$
82 molar ratio at 1:1. Standard river sand was used as the fine aggregate for mortar specimens, in
83 accordance with GB/T 14684, which was supplied by Xiamen ISO Standard Sand Co., Ltd
84 (Xiamen, China). Distilled water was used as the mixing water and a constant water-to-binder
85 (GBFS) ratio of 0.40 was fixed for the two different mixtures.



86



87

88 **Fig. 1.** Particle size distribution (a) and the morphology of the GBFS (b) used in this study.

89 **Table 1**

90 Chemical composition of the GBFS determined by X-ray fluorescence (wt.%).

Oxides	SiO ₂	CaO	Al ₂ O ₃	Fe ₂ O ₃	Na ₂ O	K ₂ O	MgO	TiO ₂	MnO	SO ₃	Others	LOI
Content	31.86	39.81	16.53	0.43	0.33	0.54	6.89	1.23	0.18	0.04	2.14	0.02

91 LOI is loss on ignition at 1000 °C.

92

93 2.2. Sample preparation

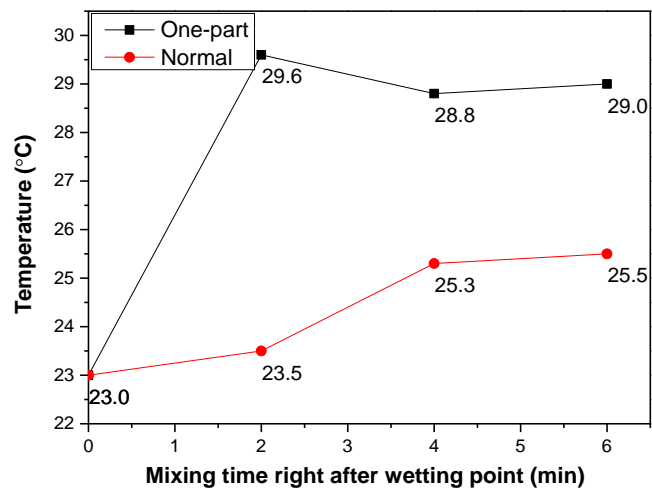
94 For the normal two-part AAS binders, the alkali-activator solution was prepared by mixing
 95 the solid sodium metasilicate fine particles with distilled water first using a magnetic stirrer
 96 and cooled off in ambient environment until reaching room temperature (23 ± 2 °C). GBFS (for
 97 pastes) or GBFS and sand (for mortars) were dry mixed for 2 min followed by adding the
 98 activator into the dry mixture with a continued mixing for 7 min prior to further procedures.
 99 For the one-part mixing, sodium metasilicate particles were directly added into the mixing bowl
 100 with pre-weighed GBFS (for pastes) and sand (for mortars), as shown in Fig. 2. Then these raw
 101 materials were dry mixed for 2 min, and the mixing water at room temperature was gradually
 102 poured with a further mixing for 7 min at low speed. After mixing, newly-mixed specimens
 103 were cast into different moulds, vibrated on a vibrating table for 30 seconds to remove air
 104 bubbles. For mortars, a part of them was used for fluidity test based on the mini-slump test. For
 105 paste slurries, they were used for setting time measurement and mineralogical as well as
 106 hydration kinetic analysis. The samples in different moulds were covered with plastic films in
 107 order to minimise moisture loss at room temperature (23 ± 2 °C) and demoulded after one day,
 108 sealed tightly in plastic bags in an ambient environment (23 ± 2 °C, RH = $50 \pm 5\%$) for different
 109 ages prior to further tests. The dosage of the solid activator powder was 7% by mass of the

110 GBFS and the sand-to-binder ratio was 2.0 for preparing mortar specimens. The detailed mix
111 proportion was determined based on our pre-tests [11, 24, 25].



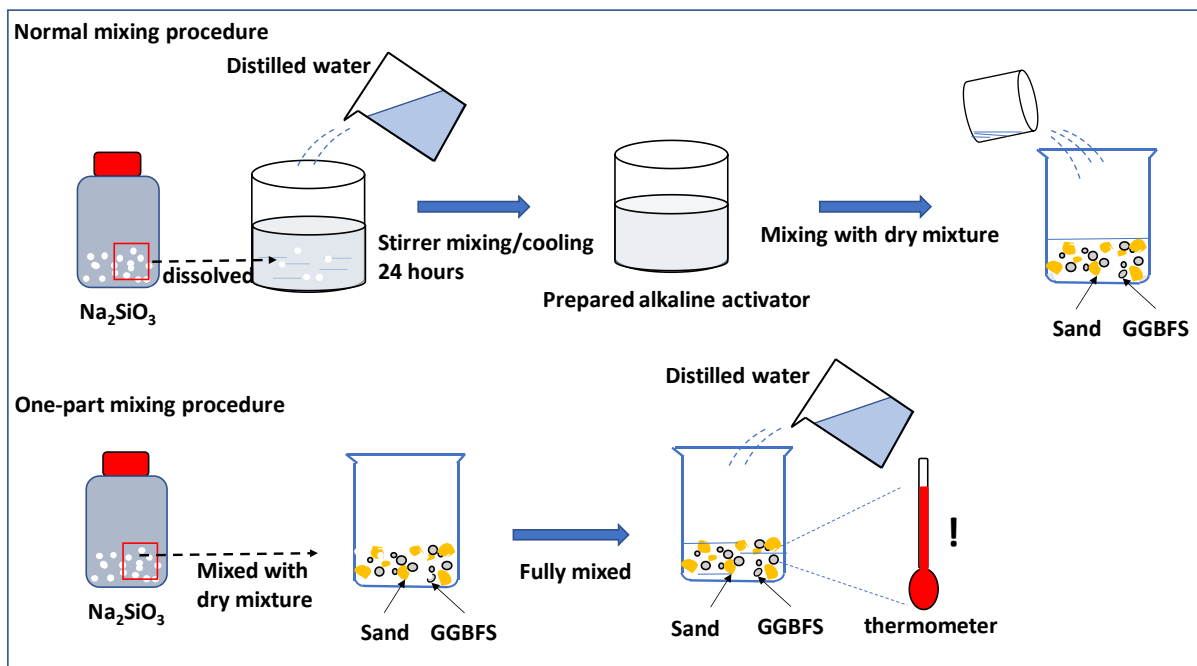
112
113 **Fig. 2.** Direct addition of sodium metasilicate particles into the dry mixture (GBFS + sand)
114 prior to the addition of distilled water into the system.

115 The temperature of the mortar specimen while mixing was measured every two minutes right
116 after the addition of the distilled water or the alkaline activator solution, which is also known
117 as wetting point (liquid comes into contact with solid materials). The corresponding value was
118 29.6 °C, 28.8 °C and 29.0 °C after 2, 4, 6 minutes of mixing for the one-part mortar specimens.
119 In comparison, for the normal specimens, the corresponding value was 23.5, 25.3 and 25.5 °C,
120 respectively. The averaged value of the three readings was 29.1 °C and 24.8 °C for the one-part
121 and normal AAS mortars accordingly. The detailed temperature changes over the mixing
122 procedure are also shown in Fig. 3. Therefore, it is apparent that one-part AAS binders had a
123 higher temperature while mixing due to the activator powder dissolution into water. The higher
124 temperature of mixing water could increase the mixture temperature, which may lead to quicker
125 water loss. A quicker water loss may then result in a higher concentration of alkalis with an
126 expected rise in pH value for those sodium metasilicate fine powders that were already
127 dissolved in the water solution [26]. A schematic presentation of the two different mixing
128 procedures, namely one-part and normal (two-part) methods, is described in Fig. 4.



129
130
131

Fig. 3. Temperature changes during the mixing procedure for one-part and the normal AAS paste specimens.



132
133
134
135

Fig. 4. Schematic presentation of the two mixing methods, namely one-part and normal mixing procedures (two-part) for the AAS mortar specimens.

136 2.3. Test procedures

137 2.3.1. Setting time, fluidity and calorimetric analysis

138 Setting time including initial and final setting time was measured using a Vicat needle based
139 on ASTM C191-19.

140 Fluidity was evaluated using mini slump test, in accordance with ASTM C1437-15. The
141 results were expressed as the averaged values of two perpendicular measurements of the spread
142 diameter for mortar binders.

143 For heat evolution measurement based on calorimetric analysis, the heat flow soon after
144 achieving the wetting point for paste slurries was captured inside an isothermal calorimeter.
145 Specifically, around 7 g slurries for the two types of pastes were filled into a glass ampoule
146 and securely sealed, followed by immediately placing into the isothermal calorimeter (TAM
147 AIR). The heat profiles over the following 96 hours were carefully monitored.

148 **2.3.2. Mechanical strength and pore-related properties**

149 The compressive strength and flexural strength in three-point bending mode was measured
150 to assess the mechanical properties of the one-part and normal AAS mortar specimens after
151 different curing ages. Prismatic samples sizing at 40 mm × 40 mm × 160 mm and cubic ones
152 with a dimension of 40 mm × 40 mm × 40 mm were used for flexural strength and compressive
153 strength, respectively. The loading rate was 2.4 kN/s for compressive strength and 50 N/s for
154 flexural strength measurement. The compressive strength was measured at the age of 1 day, 7
155 days, 28 days, 56 days and 90 days. Since the two mixtures showed rather similar compressive
156 strength in the first 7 days, the flexural strength was measured only after 7 days. Each test was
157 conducted in triplicates in accordance with ASTM C109M and the final results were the
158 average values of the three readings.

159 Pore-related properties, including water absorption and volume of permeable voids (VPV),
160 were measured in accordance to ASTM C642-06 after 28 and 56 days of curing. Samples were
161 first dried at 60 °C in a vacuum oven until constant masses were obtained (the two consecutive
162 measurements between a 24-hour interval was less than 0.5%). This drying temperature is
163 different from that suggested by ASTM C642-06, due to the potential damages caused by
164 higher temperatures on the porous microstructures of alkali-activated binders [27], as
165 previously used in other studies [5, 25].

166 Besides, the total porosity and pore-size distributions of the two types of mortar mixes after
167 56 days of curing were estimated based on nitrogen sorption test using a surface area and
168 porosity analyser (TriStar). Small fragments of untested specimens with sizes approximately
169 at 5 mm were used [28] and they were vacuum dried first at 60 °C for at least two days and then
170 degassed at 60 °C for at least 7 hours, considering many fine pores inside alkali-activated slag
171 binding systems [11, 29]. The relative pressure was 0.053-0.993 and the isotherms were
172 obtained based on Barrett-Joyner-Halenda (BJH) models. The similar sizes of the samples

173 selected were to ensure the sand in mortar specimens had no significant impact on the final
174 results.

175 **2.3.3. Mineralogical and microstructural analysis**

176 X-ray diffraction (XRD) and thermogravimetric analysis (TGA) as well as differential
177 thermogravimetry (DTG) analysis after 56 days of curing were carried out to provide
178 information on mineralogical characteristics of the paste specimens. Paste samples were first
179 finely grinded into powders (passing through 75 μm sieve) and dried at 50 °C prior to tests. For
180 XRD test, a scanning range of 5-70° (2 θ) with 0.5s/step (3183 steps in total) and a tube setting
181 of 40 kV and 40 mA were applied using a Bruker D8 Advance diffractometer. For TGA/DTG,
182 the test was performed using a thermal analyser (NETZSCH-STA 409 PG/PC) with the
183 samples heated from room temperature to 1000 °C in a nitrogen environment.

184 Scanning electron microscope (SEM) in conjunction with energy dispersive spectroscopy
185 (EDS) test was conducted on fractured paste and mortar specimens after certain curing ages
186 using a Quanta FEG 250 high resolution scanning electron microscope device. Samples after
187 the corresponding curing ages were first immersed in acetone solution to stop the hydration
188 and then dried in a vacuum oven at 50 °C for several days before the test. Finally, they were
189 mounted on a conductive adhesive and subjected to gold spraying prior to the SEM/EDS
190 detection. Secondary electron (SE) mode was employed to observe the micromorphology of
191 the products. The accelerated voltage used was 10.00 kV with a working distance of about 10
192 mm.

193

194 **3. Results and discussion**

195 **3.1. Setting time, fluidity and heat flow profile**

196 Table 2 shows the initial and final setting time of the one-part and normal AAS pastes. It is
197 apparent that the former had a much longer initial and final setting time, 123 and 310 min
198 respectively, compared to its normal counterpart (58 min and 82 min respectively). The much
199 longer setting time is possibly due to a delayed dissolution of silica and alumina species, as
200 well as the following gelation and condensation process because the sodium silicate powders
201 were mixed with dry GBFS particles first before they were dissolved in water. At the same
202 time, it is also highly possible that because of a more rapid heat release introduced by the
203 contact of sodium metasilicate with water, part of GBFS particles were dissolved at a much
204 higher rate compared to the normal mixing procedure. This partial and regional dissolution of
205 GBFS led to higher hydration process and formation of a hard reaction shell, surrounding

206 GBFS particle surfaces. This would to some extent hinder the further hydration process [30].
 207 According to the study [31], this reaction shell should be associated with the reaction among
 208 CaO (available immediately after the addition of water), soluble Si from the activator and
 209 partial Al released from the GBFS. The slower hardening rate for one-part alkali-activated blast
 210 furnace slag when using solid activator instead of the liquid one was also confirmed by Yang
 211 et al. [32] and Liu et al. [33] in which case the setting time of one-part AAS could be more than
 212 5 hours whereas the one for normal two-part AAS is only about one hour. It is worth noting
 213 that the much greater elapsed time between initial and final setting time for one-part mixing
 214 (from 123 min to 310 min) indicates that the mixture ingredients might also have changed
 215 because of the one-part mixing procedure.

216 The mini-slump test results and fluidity of the two mixes are shown in Fig. 5 and Table 2,
 217 respectively. It can be seen that the one-part mixed mortar had a similar fluidity (spread-flow
 218 = 239 mm), indicating a comparable workability as that of the normal peer (235 mm). This
 219 result suggests that although the water was added with no sodium silicate dissolved, the whole
 220 one-part mixture still displayed a homogeneous fresh state without any segregation or bleeding.
 221 Besides, the different mixing temperature seems to have a marginal effect on the fluidity [24].

222 **Table 2**

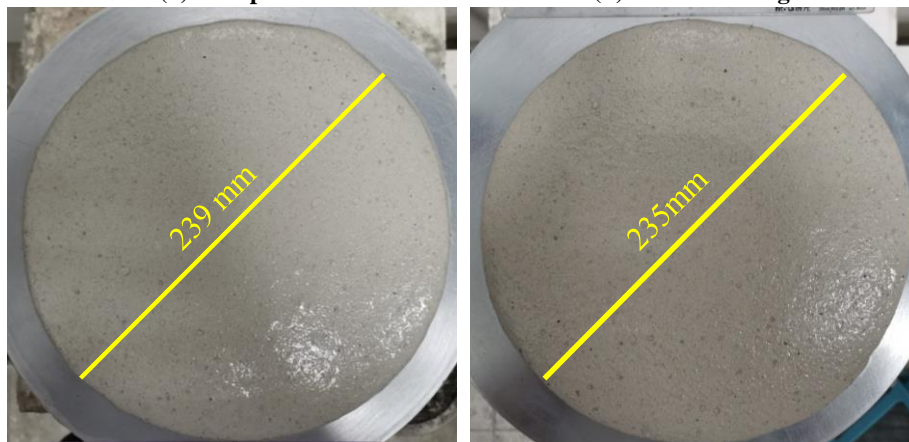
223 Initial and final setting time as well as fluidity of the two mixes of AAS specimens.

Sample types	Setting time of paste (min)		Fluidity of mortar (mm)
	Initial setting time	Final setting time	
One-part	123	310	239
Normal	58	82	235

224

(a) One-part

(b) Normal mixing



225

226

227

228

229

230

231

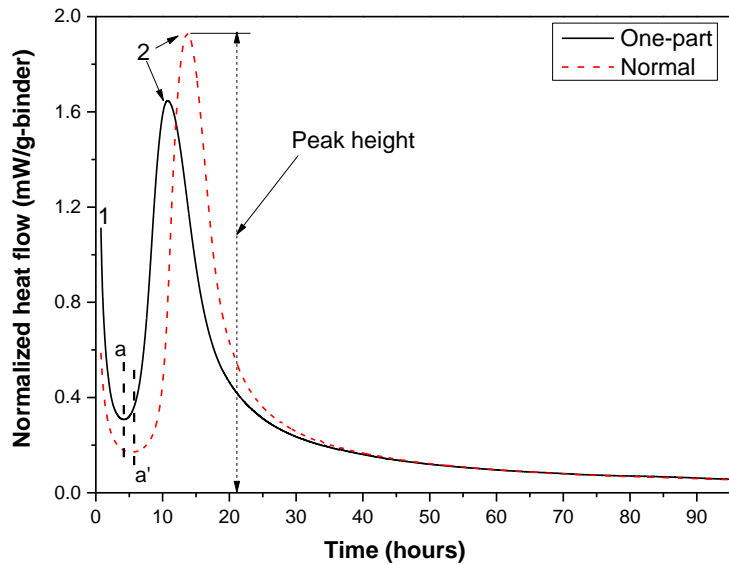
232

233 **Fig. 5.** Fluidity of the newly mixed AAS mortars, (a) one-part mixed paste and, (b) normal

234

paste.

235 The heat flow curves of the two types AAS pastes are shown in Fig. 6. The initial peaks
236 marked as '1' result from the wetting and dissolution of GBFS and the significantly higher
237 peak assigned to the one-part binder should be explained by considering the heat released from
238 the dissolution of sodium metasilicate in water, rather than the simple dissolution of GBFS in
239 the high-alkalinity activator solution. Therefore, this peak for the one-part pastes cannot imply
240 the actual starting point of the real hydration process. After this, a short induction period was
241 detected followed by an acceleration stage indicated by peak '2', which is attributed to the
242 formation of main reaction products. The starting time of the acceleration stage is marked using
243 the dashed line 'a' and 'a'' as shown in Fig. 6. Not surprisingly, the one-part paste displayed a
244 shorter induction period with an earlier commencement of the acceleration stage (shown as 'a'),
245 due in large part to the partial rapid GBFS dissolution and quicker precipitation of certain
246 reaction products on the surface of GBFS under the higher mixture temperature condition,
247 corresponding well with other literature [14, 34]. According to the study [34], the induction
248 period was even not detected because of the overlapping of the initial and acceleration peaks.
249 However, the corresponding acceleration of peak '2' is obviously lower than that of the normal
250 one. This is reasonable because some GBFS particles were covered with the hard reaction shell,
251 impeding further reaction of GBFS particles, which is consistent with the results of setting time.
252 This behaviour can be considered as 'premature' phenomenon, in which a regional rapid
253 release of heat led to a seemingly faster dissolution and reaction of GBFS at the very early
254 stage but then significantly delayed the further dissolution of GBFS particles, resulting in less
255 heat release and much prolonged setting time. In comparison, normal AAS paste displayed a
256 delayed acceleration stage, suggested by 'a'', but a much higher peak '2'. Related discussions
257 on the difference between the mechanisms of setting time and acceleration period can be found
258 in [35]. Overall, it can be concluded that the one-part mixing led to a delayed direct dissolution
259 of GBFS into activator, but the higher mixture temperature caused by the greater amount of
260 released heat to some extent counteracted this effect. This may further influence the mechanical
261 strength which is discussed in the next section.



262

263 **Fig. 6.** Heat flow curves of the two AAS pastes over 96 hours from the addition of water

264

(one-part) or alkaline solution (normal).

265

3.2. Mechanical strength and pore-related properties

266

Fig. 7 shows the compressive strength of the two AAS mortar mixes during 90 days of curing.

267

It can be seen that the compressive strength increased with time for the two types of specimens.

268

Within the 7 days of curing, there was little difference between the compressive strength of the

269

two mortar mixes, suggesting that one-part mixing had no obvious negative impact on the

270

early-age strength development up to around 7 days. As discussed before, during the early

271

stages, the similar compressive strength of the two AAS mixes can be explained by considering

272

that on the one hand, one-part mixing method led to delayed dissolution of GBFS into the

273

alkaline activator, to some extent hindering the hydration process. On the other hand, however,

274

the significantly increased temperature due to the contact of sodium metasilicate powders with

275

water partially improved the solubility and diffusivity of the GBFS in the solid-liquid system

276

[36], evidenced by the heat evolution rate as discussed earlier (Fig. 6). As a result, the latter

277

effect counteracted the delayed development of the compressive strength. Based on these

278

results, only the flexural strength since 28 days was measured because of the very similar

279

compressive strength within 7 days of curing.

280

After that, one-part mixed mortars displayed slightly lower compressive strength compared

281

to that of the normal mortar specimens up to 90 days of curing. For instance, the compressive

282

strength of the one-part mixed and normal AAS mortars was about 60.4 MPa and 67.9 MPa

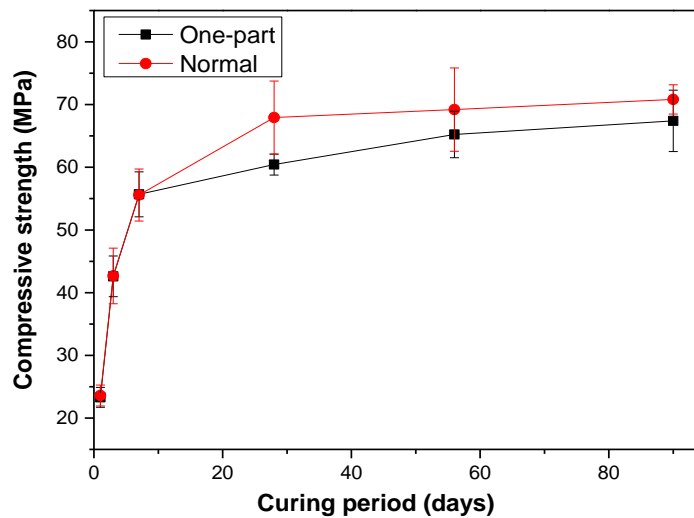
283

respectively after 28 days of curing. At 90-day of curing, the corresponding value was 67.4 and

284

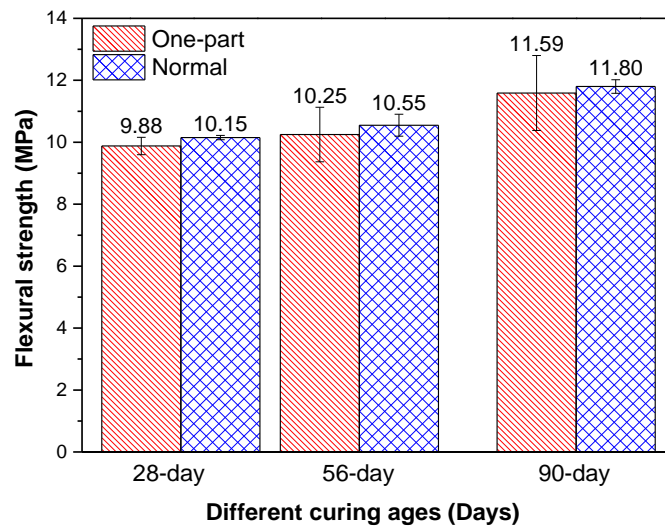
70.8 MPa. Thus, the reduction in the compressive strength for one-part mixed mortars

285 compared to normal peers was 11.04% and 4.83% after 28 days and 90 days, respectively. The
286 reduced compressive strength of one-part specimens might be associated with some intrinsic
287 defects caused by the rapid formation of hard shells around the unreacted GBFS particles
288 because of the higher mixing temperature. Similar results were also reported from other
289 researches [22, 37]. Besides, some carbonates or hydrogen carbonate phases formed in the
290 highly porous and less ordered microstructure because of the insufficient reaction could also
291 result in the degraded microstructure and hence worsened mechanical properties.



292
293 **Fig. 7.** Compressive strength of the one-part and normal AAS mortar specimens over 90 days
294 of curing.

295 The flexural strength of the two types of mortar mixes at 28-day, 56-day and 90-day of curing
296 is presented in Fig. 8. It is apparent that although normal specimens achieved slightly higher
297 flexural strength values for all the testing ages, the difference between the two mortar mixes
298 was negligible, especially considering the standard deviations for the one-part specimens. After
299 56 days of curing, for example, the flexural strength of the one-part specimen was only about
300 2.8% less than that of the normal one. These results imply that one-part mixing had no
301 significant impact on the flexural strength of the AAS mortars.



302

303 **Fig. 8.** Flexural strength of the one-part and normal AAS mortar specimens at 28, 56 and 90
 304 days of curing.

305

306 Fig. 9 shows the water absorption and volume of permeable voids (VPV) of the one-part and
 307 normal AAS mortar specimens after 28 and 56 days of curing. It can be seen that the water
 308 absorption and VPV decreased as the curing time increased from 28 days to 56 days, regardless
 309 of mortar mixes [38]. Besides, after 28 days of curing, the water absorption and VPV was 3.94%
 310 and 7.34% respectively for the one-part mortar specimens, whereas the corresponding values
 311 for the normal mortar was 4.19% and 7.71%. The values for the one-part mortar were similar
 312 to the data obtained in another literature [39]. Surprisingly, the one-part mortars gained lower
 313 water absorption and VPV, indicating a more densified microstructure in comparison to the
 314 normal mortar specimens after 28 days. However, after 56 days, the water absorption and VPV
 315 for the one-part mortars was 3.73% and 6.51% respectively, higher than those of the normal
 316 mortars. A higher porosity suggested by higher water absorption and VPV usually leads to
 317 lower compressive strength at later curing ages [40]. Hence, the 56-day results are in line with
 318 the mechanical strength, whereas the reduced 28-day compressive strength but lower water
 319 absorption and VPV for one-part mortars indicates that some other factors such as the loading
 320 capacity of the binding gels, any defects and/or precipitations may adversely influence the
 321 overall results [41].

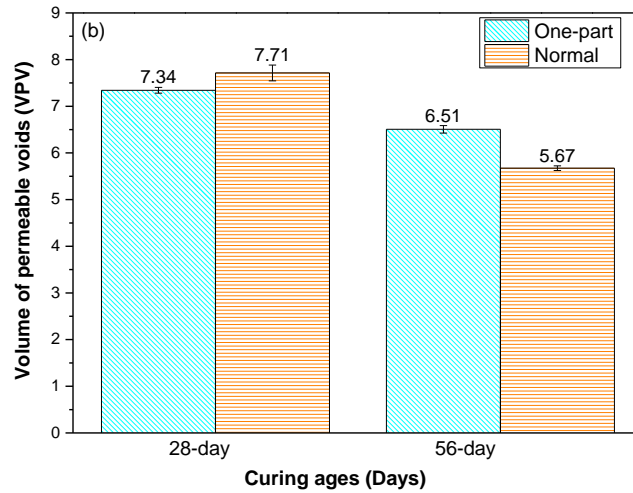
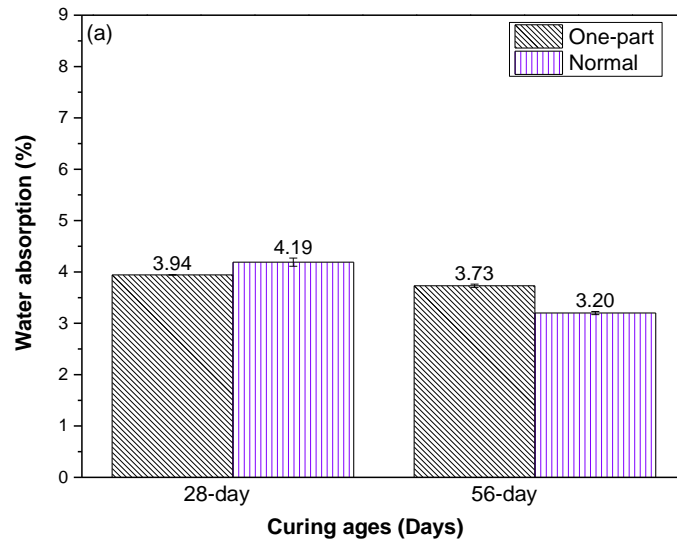
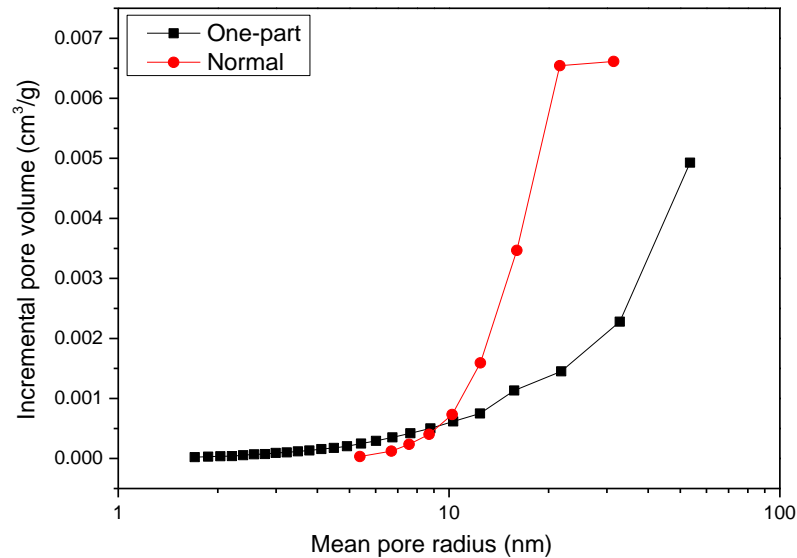


Fig. 9. Water absorption (a) and volume of permeable voids (b) of the two AAS mortar specimens after 28 days and 56 days of curing.

Different pore-size distributions for nanopores obtained from the nitrogen absorption test are shown in Fig. 10. Pores smaller than 50 nm in diameter can be categorized as gel pores, indicating the presence of alkali-activated gel products, such as C-A-S-H gels [42]. It seems that one-part mixed mortars had a lower volume of mesopores (less than 50 nm) compared to the normal peers, which suggests reduced degree of alkali activation and hence fewer C-A-S-H gels as compared to the normal AAS counterpart [21]. This was also evidenced by the lower surface area of the one-part specimens, which was only 3.788 m²/g compared to 4.268 m²/g for the normal peer. Fewer C-A-S-H gels would then result in lower compressive strength as the C-A-S-H gels are the main strength contributor to the AAS systems, in line with the compressive strength as shown in Fig. 7. Providing the higher water absorption and VPV (Fig.

337 9) but lower volume of mesopores in the one-part mortar specimens (Fig. 10), it can be inferred
 338 that this type of specimens had a greater amount of harmful pores (50-200 nm) and/or more-
 339 harmful pores (>200 nm) [43]. As a result, one-part specimens might have a poorer durability
 340 performance in comparison to the normal AAS specimens, which needs further investigations.



341
 342 **Fig. 10.** Pore volume distribution of the one-part AAS and normal mortars after 56 days of
 343 curing.

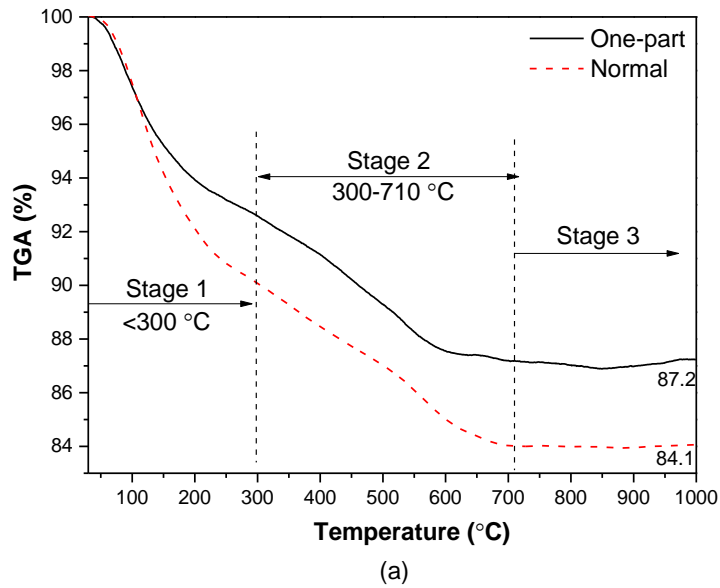
345 3.3. Mineralogical and microstructural analysis

346 3.3.1. TGA/DTG

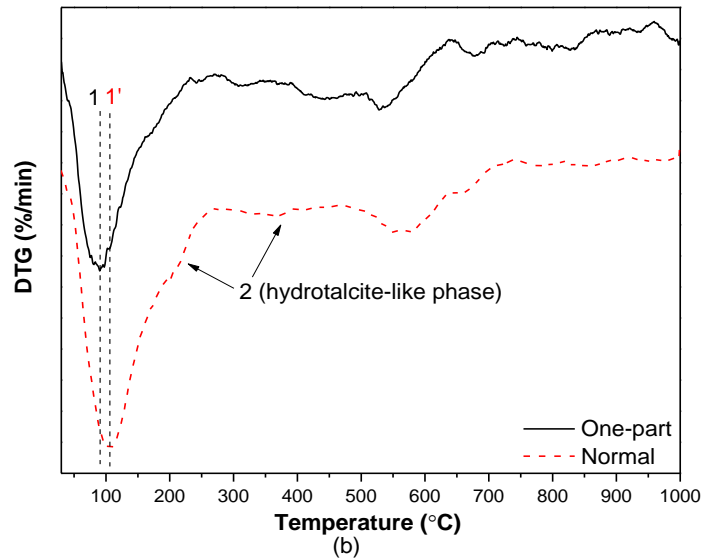
347 The relative gel content in the one-part and normal AAS pastes can be reflected by TGA and
 348 DTG curves, as shown in Fig. 11(a) and (b). For AAS binders, there are three stages of mass
 349 changes in TGA curves: i) the first stage up to 300 °C is assigned to the mass loss of free and
 350 bound water from C-A-S-H gels [44]; ii) the second stage from 300-710 °C is mainly attributed
 351 to chemically-bonded water loss and dehydroxylation of hydrotalcite-like phases [6, 45], loss
 352 of CO₂ from vaterite [46] or decomposition of calcite between 670 and 710 °C [47]; iii) the
 353 third stage above 710 °C is influenced by the decomposition of other calcite [46] and transitions
 354 of C-S-H and/or C-(A)-S-H to some crystalline phases [48]. The mass loss during the first stage
 355 can be used to quantify the degree of hydration since it is closely associated with the C-(A)-S-
 356 H gels. Specifically, the corresponding total mass loss within ‘Stage 1’ was 7.4% and 10.0%
 357 for the one-part and normal AAS pastes respectively. Thus, it shows that the former had fewer
 358 C-A-S-H gels than that of the normal mortar, corresponding well with the nitrogen adsorption

359 test results. Moreover, the total mass loss was 12.8% and 15.9% respectively, suggesting that
360 the geopolymerisation process of one-part paste was not as complete as the normal counterpart.

361 For DTG, the decreased intensity of the endothermic peak assigned to the dehydration of C-
362 (A)-S-H in the one-part AAS paste compared to the normal paste also suggests that the amount
363 of C-(A)-S-H gel in the former was less. Moreover, the lower temperature marked as '1' at
364 around 90 °C than that of the normal paste (denoted as '1' at around 100 °C) indicates a more
365 densified structure of C-(A)-S-H in the normal AAS paste. Therefore, it seems that one-part
366 mixing not only led to reduced amount of the main hydration products due in large part to the
367 limited dissolution of GBFS, but may also negatively influence the polycondensation process
368 and the resultant microstructures of the C-(A)-S-H gels. This is reasonable because for the one-
369 part mixed specimens, the amount of available Al is less owing to the delayed dissolution of
370 GBFS (the sole source of Al) into the alkaline activator. Hence, the structure of the binder was
371 relatively weaker compared to the normal paste with higher amount of available alumina [49].
372 Besides, the weak shoulder at 220-230 °C and the small mass loss between 350 and 400 °C,
373 highlighted as '2' in the XRD pattern of the normal AAS paste, can be assigned to the presence
374 of hydrotalcite-like phases [50, 51]. Thus, it is concluded that the one-part sample contained
375 no hydrotalcite-like phases. This result corresponds well with other results implying that high-
376 temperature or subzero temperature (-5, -10 and even -20 °C) would all lead to the absence of
377 hydrotalcite phase because when the temperature is too high or too low, the depolymerisation
378 and polycondensation process would be adversely affected [14, 18, 21, 30]. In this study, the
379 temperature of the one-part mixing is too high (Fig. 3), as mentioned earlier to explain the
380 prolonged setting time, thus delaying the subsequent reaction process. In comparison, room
381 temperature (23 °C) or 0 °C could result in the formation of hydrotalcite [14, 20].



382



383

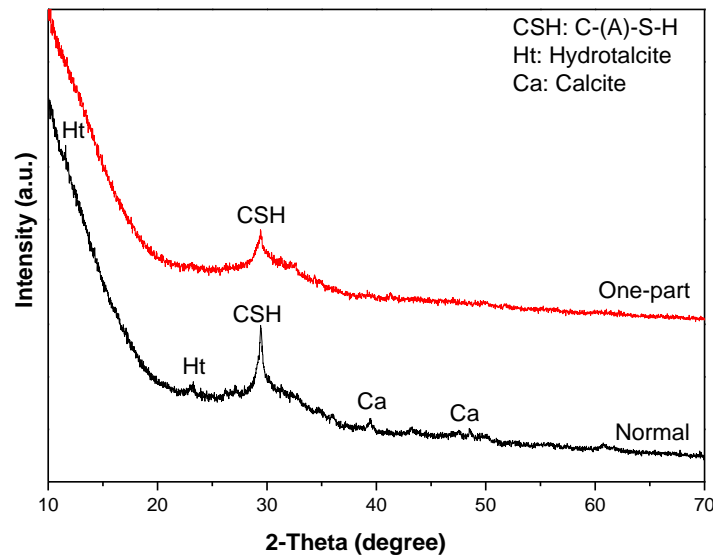
384 **Fig. 11.** (a) Thermogravimetric analysis (TGA); (b) differential thermogravimetry analysis
 385 (DTG) of the one-part and normal AAS paste samples after 56 days of curing.

386

387 3.3.2. XRD results

388 According to the XRD patterns in Fig. 12, the similar broad peaks at around $29^\circ 2\theta$ for the
 389 two AAS mixes can be assigned to the main hydration product, namely C-(A)-S-H gels, which
 390 is in agreement with other studies [14, 46, 52]. Besides, the relative intensity of this peak for
 391 the one-part specimen is lower compared to that for the normal specimen, implying that one-
 392 part mixing led to the less formation hydration products, consistent with the TG/DTG results
 393 and the lower compressive strength after 56 days of curing (shown in Fig. 7). In addition,
 394 normal specimens also displayed some typical peaks that belong to hydrotalcite

395 $(Mg_6Al_2CO_3(OH)_{16} \cdot 4H_2O)$, indicating that there was some hydrotalcite formed in the normal
396 specimens after 56 days. The formation of hydrotalcite often occurs when the content of MgO
397 is more than 5 wt.% (as shown in Table 1) [20], corresponding well with the DTG curve as
398 shown in Fig. 11(b). In addition, there are some traces of calcite evidenced by the two small
399 diffraction peaks, which could be due to the carbonation of C-(A)-S-H gels [53].



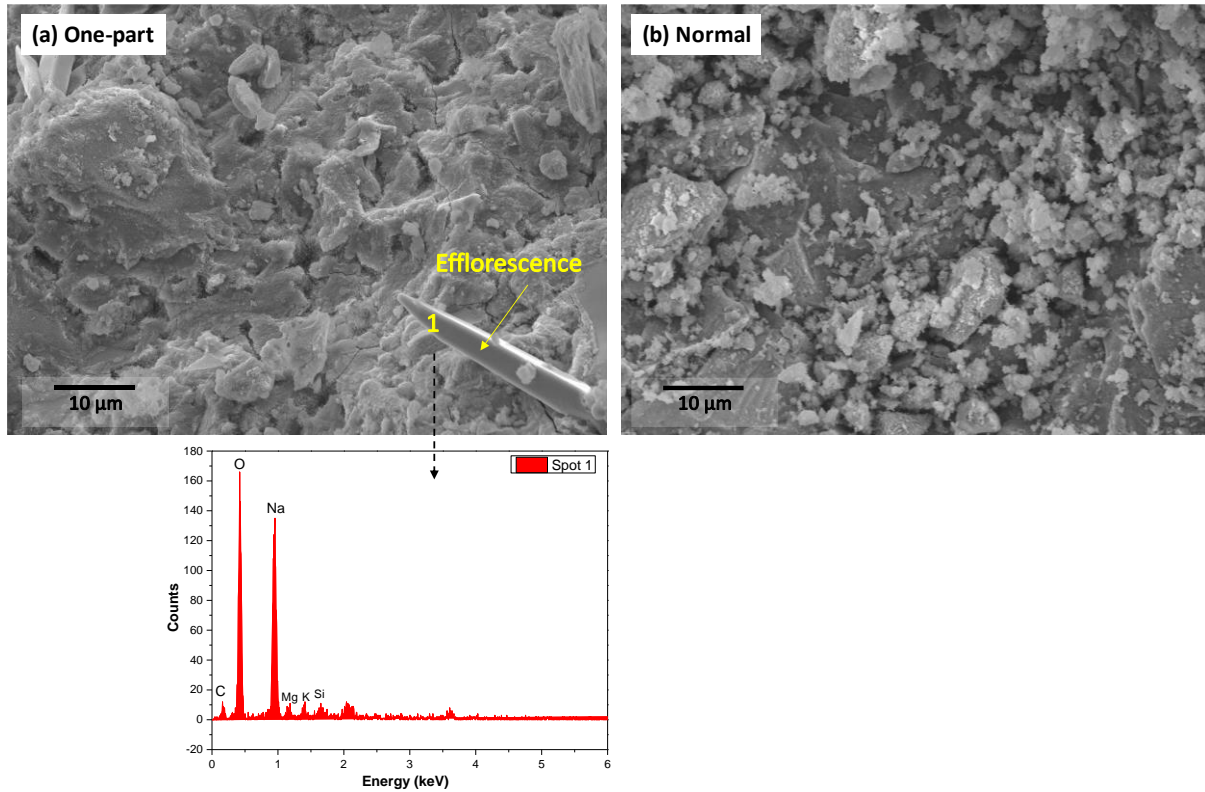
400

401 **Fig. 12.** X-ray diffraction patterns of the one-part and normal mixing AAS paste powders
402 after 56 days of curing.

403 3.3.3. SEM/EDS

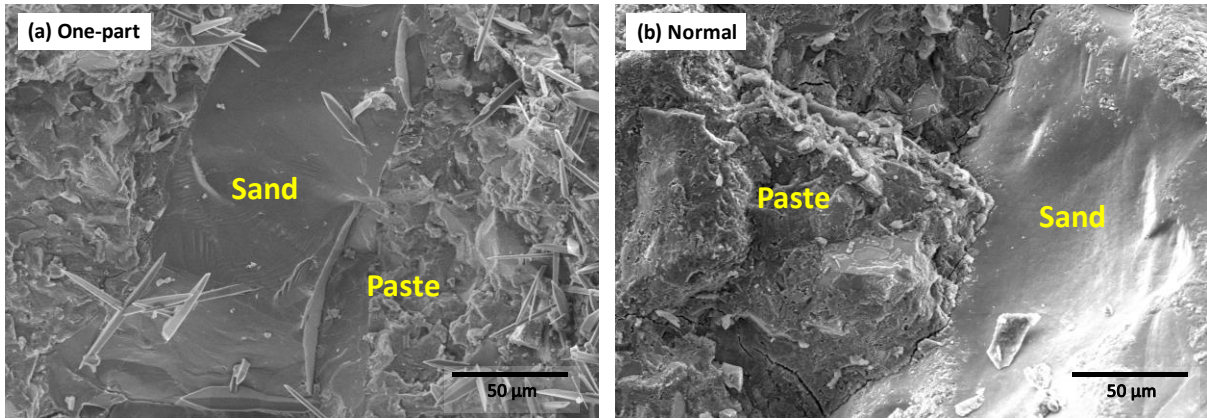
404 The morphology observations of the two types of AAS pastes and mortars are shown in Fig.
405 13 and Fig. 14, respectively. Based on Fig. 13, it can be seen that there are some crystals on
406 the surface of the one-part AAS paste specimens which might be due to efflorescence.
407 According to the EDS analysis, the crystals should be hydrated sodium carbonate
408 $(Na_2CO_3 \cdot nH_2O)$ as the crystal is rich in Na, O and C [54], presented also in Fig. 13. In
409 comparison, there is no efflorescence phenomenon for the normal AAS pastes. Considering
410 that the efflorescence is highly dependent on the pores which act as a leaching channel [54, 55],
411 this difference might be due to the fact that one-part specimens had more interconnected open
412 pores since there was not enough C-A-S-H gels formed in the binding matrix. Moreover, the
413 partial consumption of alkalis due to the local fast chemical reaction would lead to more
414 available Na^+ ions in the pore solution. As a result, more free alkalis could travel through the
415 porous systems to the surface of the samples. In contrast, normal AAS binders were more
416 densified because of the physical compaction by different hydration products, as evidenced by
417 the TG/DTG and XRD results. This result implies that one-part specimens are more prone to

418 efflorescence compared to its normal counterpart. Nonetheless, it should be noted that the
419 amount of sodium carbonate is limited, since little signal of it was detected by DTG and XRD.
420 Therefore, Fig. 13 does not lead to a firm conclusion that one-part AAS is subject to severe
421 risk of efflorescence, rather it gives an indication that the efflorescence of one-part AAS might
422 deserve further attention.



423
424 **Fig. 13.** SEM images (5000 × magnification) and EDS analysis of (a) one-part and (b) normal
425 AAS paste specimens after 56 days of curing.

426 For mortar specimens, it can be seen that both two types of AAS mortars are compact
427 including both paste and interfacial transition zone between the paste and sand particles, except
428 some sharp crystals observed on the surface of the one-part mixed binding matrix. Therefore,
429 the slightly lower mechanical strength might be associated with the presence of these small
430 crystalline phases and/or some intrinsic defects as well as fewer C-(A)-S-H gels caused by the
431 incomplete dissolution and reaction of GBFS particles in some regions of the binder because
432 of the one-part mixing. Since paste samples were used in XRD and TGA tests, these crystals
433 in ITZ region were not indicated in those tests. Polished samples with immersion of epoxy
434 should be used to further investigate the properties of ITZ of AAS.



435

436

437

Fig. 14. SEM images (1500 × magnification) of (a) one-part and (b) normal AAS mortar specimens after 56 days of curing.

438

4. Conclusions

439

440

441

This study investigated both fresh and hardened properties of one-part and normal AAS binders activated by sodium metasilicate. According to the experimental results, several conclusions can be summarised as follows:

442

443

444

445

- Both the initial and final setting time was significantly prolonged for the one-part AAS binders compared to the normal counterpart due probably to the hard reaction shell formed under the condition of regional high rate of dissolution of GBFS owing to the rapid release of heat.

446

447

448

449

450

451

- One-part AAS mortars displayed slightly lower later-stage compressive strength than that of the normal counterparts but achieved similar values of compressive strength within about 7 days of curing. This can also be explained by considering the higher rate of dissolution of GBFS in some regions as evidenced by the early starting point of the acceleration stage in the heat evolution curves but overall a delayed and incomplete reaction of GBFS.

452

453

454

- One-part specimens had higher porosity evidenced by larger water absorption and VPV, but lower volume of mesopores, indicating that there should be more harmful pores which might affect the durability of these binders.

455

456

457

458

459

- The absence of hydrotalcite formed and fewer C-(A)-S-H gels for the one-part AAS binders correspond well with the delayed and incomplete hydration of GBFS suggested by other tests, which is closely associated with higher mixing temperature. Besides, one-part AAS binders seem to be more prone to efflorescence, evidenced by the crystals in the morphological and elemental analysis.

460 In general, it is feasible to use AAS binders given the similar fluidity and compressive
461 strength as well as flexural strength. However, the much delayed hardening process, low degree
462 of alkali activation of slags and high risks of efflorescence need extra focus.

463

464 **Conflict of interest**

465 The authors declare that they have no known competing financial interests or personal
466 relationships that may influence the work reported in this paper.

467

468 **Acknowledgements**

469 This research work was financially supported by the National Natural Science Foundation of
470 China (Grant Nos. 51878412, 51520105012, 51878413, and 51678368), the Shenzhen R&D
471 Fund (Grant No. JCYJ20190808112019066), and the Guangdong Provincial Key Laboratory
472 of Durability for Marine Civil Engineering (SZU) (Grant No. 2020B1212060074). Besides,
473 Instrumental Analysis Center of Shenzhen University is also acknowledged.

474

475 **References**

- 476 [1] R.M. Andrew, Global CO₂ emissions from cement production, *Earth Syst. Sci. Data.*
477 *Discuss.* (2017).
- 478 [2] S. Zhang, A. Keulen, K. Arbi, G. Ye, Waste glass as partial mineral precursor in alkali-
479 activated slag/fly ash system, *Cement and Concrete Research* 102 (2017) 29-40.
- 480 [3] S.-L. Zhang, X.-Q. Qi, S.-Y. Guo, J. Ren, J.-C. Chen, B. Chi, X.-C. Wang, Effect of a novel
481 hybrid TiO₂-graphene composite on enhancing mechanical and durability characteristics of
482 alkali-activated slag mortar, *Construction and Building Materials* 275 (2021) 122154.
- 483 [4] J. Ren, L. Zhang, R. San Nicolas, Degradation of alkali-activated slag/fly ash mortars under
484 different aggressive acid conditions, *Journal of materials in civil engineering* (2020).
- 485 [5] J. Ren, S. Guo, J. Su, T. Zhao, J. Chen, S. Zhang, A novel TiO₂/Epoxy resin composited
486 geopolymer with great durability in wetting-drying and phosphoric acid solution, *Journal of*
487 *Cleaner Production* 227 (2019) 849-860.
- 488 [6] M.S. Kim, Y. Jun, C. Lee, J.E. Oh, Use of CaO as an activator for producing a price-
489 competitive non-cement structural binder using ground granulated blast furnace slag, *Cement*
490 *and Concrete Research* 54 (2013) 208-214.
- 491 [7] P. Sargent, P.N. Hughes, M. Rouainia, A new low carbon cementitious binder for stabilising
492 weak ground conditions through deep soil mixing, *Soils and Foundations* 56(6) (2016) 1021-
493 1034.
- 494 [8] C. Shi, B. Qu, J.L. Provis, Recent progress in low-carbon binders, *Cement and Concrete*
495 *Research* 122 (2019) 227-250.
- 496 [9] T. Bakharev, J.G. Sanjayan, Y.B. Cheng, Sulfate attack on alkali-activated slag concrete,
497 *Cement and Concrete Research* 32(2) (2002) 211-216.
- 498 [10] M. Albitar, M.M. Ali, P. Visintin, M. Drechsler, Durability evaluation of geopolymer and
499 conventional concretes, *Construction and Building Materials* 136 (2017) 374-385.

- 500 [11] J. Ren, L. Zhang, R. San Nicolas, Degradation process of alkali-activated slag/fly ash and
501 Portland cement-based pastes exposed to phosphoric acid, *Construction and Building Materials*
502 232 (2020) 117209.
- 503 [12] D.L. Kong, J.G. Sanjayan, Effect of elevated temperatures on geopolymer paste, mortar
504 and concrete, *Cement and concrete research* 40(2) (2010) 334-339.
- 505 [13] A. Adam, Strength and durability properties of alkali activated slag and fly ash-based
506 geopolymer concrete, School of Civil, Environmental and Chemical Engineering, RMIT
507 University, 2009.
- 508 [14] M. Almahadmeh, A.M. Soliman, Effects of mixing water temperatures on properties of
509 one-part alkali-activated slag paste, *Construction and Building Materials* 266 (2021) 121030.
- 510 [15] W. Chen, R. Peng, C. Straub, B. Yuan, Promoting the performance of one-part alkali-
511 activated slag using fine lead-zinc mine tailings, *Construction and Building Materials* 236
512 (2020) 117745.
- 513 [16] B. Yang, J.G. Jang, Environmentally benign production of one-part alkali-activated slag
514 with calcined oyster shell as an activator, *Construction and Building Materials* 257 (2020)
515 119552.
- 516 [17] T. Luukkonen, Z. Abdollahnejad, J. Yliniemi, P. Kinnunen, M. Illikainen, One-part alkali-
517 activated materials: A review, *Cement and Concrete Research* 103 (2018) 21-34.
- 518 [18] K. Wang, P.N. Lemougna, Q. Tang, W. Li, Y. He, X. Cui, Low temperature
519 depolymerization and polycondensation of a slag-based inorganic polymer, *Ceramics*
520 *International* 43(12) (2017) 9067-9076.
- 521 [19] Y.-m. Gu, Y.-h. Fang, D. You, Y.-f. Gong, C.-h. Zhu, Properties and microstructure of
522 alkali-activated slag cement cured at below- and about-normal temperature, *Construction and*
523 *Building Materials* 79 (2015) 1-8.
- 524 [20] T. Luukkonen, Z. Abdollahnejad, J. Yliniemi, P. Kinnunen, M. Illikainen, Comparison of
525 alkali and silica sources in one-part alkali-activated blast furnace slag mortar, *Journal of*
526 *Cleaner Production* 187 (2018) 171-179.
- 527 [21] A. Alzaza, K. Ohenoja, M. Illikainen, One-part alkali-activated blast furnace slag for
528 sustainable construction at subzero temperatures, *Construction and Building Materials* 276
529 (2021) 122026.
- 530 [22] B. Nematollahi, J. Sanjayan, F.U.A. Shaikh, Synthesis of heat and ambient cured one-part
531 geopolymer mixes with different grades of sodium silicate, *Ceramics International* 41(4) (2015)
532 5696-5704.
- 533 [23] M.X. Peng, Z.H. Wang, S.H. Shen, Q.G. Xiao, Synthesis, characterization and
534 mechanisms of one-part geopolymeric cement by calcining low-quality kaolin with alkali,
535 *Materials and Structures* 48(3) (2015) 699-708.
- 536 [24] J. Ren, H. Sun, K. Cao, Z. Ren, B. Zhou, W. Wu, F. Xing, Effects of natural seawater
537 mixing on the properties of alkali-activated slag binders, *Construction and Building Materials*
538 294 (2021) 123601.
- 539 [25] J. Ren, S. Guo, T. Zhao, J. Chen, R. San Nicolas, L. Zhang, Constructing a novel nano-
540 TiO₂/Epoxy resin composite and its application in alkali-activated slag/fly ash pastes,
541 *Construction and Building Materials* 232 (2020) 117218.
- 542 [26] B. Yuan, Q.L. Yu, H.J.H. Brouwers, Time-dependent characterization of Na₂CO₃
543 activated slag, *Cement and Concrete Composites* 84 (2017) 188-197.
- 544 [27] I. Ismail, S.A. Bernal, J.L. Provis, S. Hamdan, J.S. van Deventer, Drying-induced changes
545 in the structure of alkali-activated pastes, *Journal of Materials Science* 48(9) (2013) 3566-3577.
- 546 [28] J. Xing, Y. Zhao, J. Qiu, X. Sun, Microstructural and Mechanical Properties of Alkali
547 Activated Materials from Two Types of Blast Furnace Slags, *Materials (Basel, Switzerland)*
548 12(13) (2019).

549 [29] Z. Li, M. Nedeljković, B. Chen, G. Ye, Mitigating the autogenous shrinkage of alkali-
550 activated slag by metakaolin, *Cement and Concrete Research* 122 (2019) 30-41.

551 [30] B.S. Gebregziabher, R.J. Thomas, S. Peethamparan, Temperature and activator effect on
552 early-age reaction kinetics of alkali-activated slag binders, *Construction and Building*
553 *Materials* 113 (2016) 783-793.

554 [31] F. Matalkah, L. Xu, W. Wu, P. Soroushian, Mechanochemical synthesis of one-part alkali
555 aluminosilicate hydraulic cement, *Materials and Structures* 50(1) (2016) 97.

556 [32] K.-H. Yang, J.-K. Song, A.F. Ashour, E.-T. Lee, Properties of cementless mortars
557 activated by sodium silicate, *Construction and Building Materials* 22(9) (2008) 1981-1989.

558 [33] C. Liu, X. Yao, W. Zhang, Controlling the setting times of one-part alkali-activated slag
559 by using honeycomb ceramics as carrier of sodium silicate activator, *Construction and Building*
560 *Materials* 235 (2020) 117091.

561 [34] W. Almakhadmeh, A.M. Soliman, COMPARATIVE ANALYSIS OF REACTION
562 KINETICS OF ONE AND TWO PARTS ALKALI ACTIVATED SLAG, CSCE Annual
563 Conference, Laval (Greater Montreal), 2019.

564 [35] Z. Li, T. Lu, X. Liang, H. Dong, G. Ye, Mechanisms of autogenous shrinkage of alkali-
565 activated slag and fly ash pastes, *Cement and Concrete Research* 135 (2020) 106107.

566 [36] Gruskovnjak, A., Lothenbach, B., Holzer, L., Figi, R., Winnefeld, F., Hydration of alkali-
567 activated slag: comparison with ordinary Portland cement, *Advances in Cement Research*
568 (2006).

569 [37] B. Nematollahi, J. Sanjayan, Ambient temperature cured one-part engineered geopolymer
570 composite: a sustainable alternative to engineered cementitious composite, 9th Rilem
571 International Symposium on Fiber Reinforced Concrete, 2016.

572 [38] J.L. Provis, R.J. Myers, C.E. White, V. Rose, J.S. van Deventer, X-ray microtomography
573 shows pore structure and tortuosity in alkali-activated binders, *Cement and Concrete Research*
574 42(6) (2012) 855-864.

575 [39] P. Perumal, H. Sreenivasan, T. Luukkonen, A.M. Kantola, V.-V. Telkki, P. Kinnunen, M.
576 Illikainen, High strength one-part alkali-activated slag blends designed by particle packing
577 optimization, *Construction and Building Materials* 299 (2021) 124004.

578 [40] M.A. Megat Johari, J.J. Brooks, S. Kabir, P. Rivard, Influence of supplementary
579 cementitious materials on engineering properties of high strength concrete, *Construction and*
580 *Building Materials* 25(5) (2011) 2639-2648.

581 [41] A. Younis, U. Ebead, P. Suraneni, A. Nanni, Fresh and hardened properties of seawater-
582 mixed concrete, *Construction and Building Materials* 190(NOV.30) (2018) 276-286.

583 [42] Sindhunata, J.L. Provis, G.C. Lukey, H. Xu, J.S.J. van Deventer, Structural Evolution of
584 Fly Ash Based Geopolymers in Alkaline Environments, *Industrial & Engineering Chemistry*
585 *Research* 47(9) (2008) 2991-2999.

586 [43] M.-h. Zhang, H. Li, Pore structure and chloride permeability of concrete containing nano-
587 particles for pavement, *Construction and Building Materials* 25(2) (2011) 608-616.

588 [44] D. Shi, Y. Yao, J. Ye, W. Zhang, Effects of seawater on mechanical properties, mineralogy
589 and microstructure of calcium silicate slag-based alkali-activated materials, *Construction and*
590 *Building Materials* 212 (2019) 569-577.

591 [45] N. Mobasher, S.A. Bernal, J.L. Provis, Structural evolution of an alkali sulfate activated
592 slag cement, *Journal of Nuclear Materials* 468 (2016) 97-104.

593 [46] U. De Filippis, E. Prud'homme, S. Meille, Relation between activator ratio, hydration
594 products and mechanical properties of alkali-activated slag, *Construction and Building*
595 *Materials* 266 (2021) 120940.

596 [47] N. Yang, W. Yue, *The Handbook of Inorganic Metalloid Materials Atlas (in Chinese)*,
597 Wuhan University of Technology Press 2000.

598 [48] N.K. Lee, K.T. Koh, G.H. An, G.S. Ryu, Influence of binder composition on the gel
599 structure in alkali activated fly ash/slag pastes exposed to elevated temperatures, *Ceramics*
600 *International* 43(2) (2017) 2471-2480.

601 [49] E. Najafi Kani, A. Allahverdi, J.L. Provis, Efflorescence control in geopolymer binders
602 based on natural pozzolan, *Cement and Concrete Composites* 34(1) (2012) 25-33.

603 [50] O. Burciaga-Díaz, I. Betancourt-Castillo, Characterization of novel blast-furnace slag
604 cement pastes and mortars activated with a reactive mixture of MgO-NaOH, *Cement and*
605 *Concrete Research* 105 (2018) 54-63.

606 [51] M. Ben Haha, G. Le Saout, F. Winnefeld, B. Lothenbach, Influence of activator type on
607 hydration kinetics, hydrate assemblage and microstructural development of alkali activated
608 blast-furnace slags, *Cement and Concrete Research* 41(3) (2011) 301-310.

609 [52] J. Zhang, C. Shi, Z. Zhang, Z. Ou, Durability of alkali-activated materials in aggressive
610 environments: A review on recent studies, *Construction and Building Materials* 152 (2017)
611 598-613.

612 [53] R.J. Myers, E. L'Hôpital, J.L. Provis, B. Lothenbach, Effect of temperature and aluminium
613 on calcium (alumino)silicate hydrate chemistry under equilibrium conditions, *Cement and*
614 *Concrete Research* 68 (2015) 83-93.

615 [54] Z. Zhang, J.L. Provis, A. Reid, H. Wang, Fly ash-based geopolymers: the relationship
616 between composition, pore structure and efflorescence, *Cement and Concrete Research* 64
617 (2014) 30-41.

618 [55] P. Zhang, Q.-F. Li, Durability of high performance concrete composites containing silica
619 fume, *Proceedings of the Institution of Mechanical Engineers, Part L: Journal of Materials*
620 *Design and Applications* 227 (2013) 343-349.

621